

File ID uvapub:2516
Filename 25195y.pdf
Version unknown

SOURCE (OR PART OF THE FOLLOWING SOURCE):

Type article
Title Hyperbolicity and critical points in two-moment approximative radiative
 transfer
Author(s) J.M. Smit
Faculty FNWI: Institute for Theoretical Physics (ITF)
Year 1997

FULL BIBLIOGRAPHIC DETAILS:

<http://hdl.handle.net/11245/1.132606>

Copyright

It is not permitted to download or to forward/distribute the text or part of it without the consent of the author(s) and/or copyright holder(s), other than for strictly personal, individual use, unless the work is under an open content licence (like Creative Commons).

Hyperbolicity and critical points in two-moment approximate radiative transfer

J.M. Smit¹, J.Cernohorsky², and C.P. Dullemond³

¹ Center for High Energy Astrophysics (CHEAF), Kruislaan 403, 1098 SJ, Amsterdam, The Netherlands

² Deutsche Morgan Grenfell, Global FX Options, 6-8 Bishopsgate, EC2P 2AT, London, UK

³ Leiden Observatory, P.O. Box 9513, 2300 RA Leiden, The Netherlands

Received 23 December 1996 / Accepted 6 March 1997

Abstract. We present numerical calculations of spherically symmetric radiative transport using a two-moment (P-1) method with a two-dimensional non-linear closure on the Eddington factor. The stationary state solutions contain a critical point. We demonstrate that the two-moment equations with a non-linear closure are well behaved. The solutions are physically acceptable, regular and accurate.

Key words: radiative transfer – methods: numerical – stars: general – stars: supernovae: general

1. Introduction

In practical calculations of radiation transport, solving the full transport equation is often too costly. This is for example the case in numerical simulations of supernova explosions and the early neutrino driven neutron star formation and cooling phase, in which neutrino transport is coupled to a dynamically evolving stellar environment. An approximate approach that reduces the dimensionality of the transfer problem is the P-N method (Pomraning 1973). In the P-N, or “moment method”, one takes angular moments of the transport equation, resulting in an infinite set of moment equations. For practical purposes this infinite hierarchy is truncated at a certain level by making a plausible closure assumption. The widely used scheme that we consider here is the P-1, or two-moment approximation, with a closure on the second angular moment of the radiation field (which is the same as using a variable Eddington factor).

We consider the monochromatic transport equation for a spherically symmetric system, a static matter background in Newtonian gravity, excluding inelastic and anisotropic scattering processes, and using natural units $c = 1$. The transport equation reads

$$\partial_t F + \mu \partial_r F + \frac{1 - \mu^2}{r} \partial_\mu F = \kappa_a (B - F) + \kappa_s (J - F) \quad (1)$$

It contains the distribution function $F(r, \mu, t)$, the inverse absorption and (isotropic) scattering mean free paths κ_a and κ_s respectively, the equilibrium distribution B and the first angular moment J , defined below in Eq. (4). The first two moment equations are obtained by multiplying Eq. (1) by 1 and μ respectively and integrating over μ . This gives

$$\partial_t J + \frac{1}{r^2} \partial_r (r^2 H) = \kappa_a (B - J) \quad , \quad (2)$$

and

$$\partial_t H + \frac{1}{r^2} \partial_r (r^2 K) + \frac{K - J}{r} = -(\kappa_a + \kappa_s) H \quad , \quad (3)$$

with the standard definitions

$$\{J, H, K\} \equiv \frac{1}{2} \int_{-1}^{+1} d\mu \mu^{\{0,1,2\}} F \quad . \quad (4)$$

The two moment equations (2) and (3) basically express the conservation of energy and momentum with the three angular moments J , H and K of the radiation field proportional to the radiation energy density, flux and pressure. Higher angular moments of the radiation field and the transport equation, arising in the P-N approximation, have no simple physical interpretation.

The closure is achieved by a prescription

$$K = K(J, H) \quad . \quad (5)$$

In analogy with an equation of state in hydrodynamics it can be constructed in different ways, and is usually adapted to fit the geometry of the problem. Our interest is in the situation where an opaque region is surrounded by an extended atmosphere. In the opaque region the mean free path is short compared with the typical length scale of the system, and we have $K/J \rightarrow 1/3$. Far out in the transparent zones the radiation becomes very forwardly peaked and $K/J \rightarrow 1$, $H/J \rightarrow 1$. The closure must meet with these two limits in order to be able to describe the radiation field throughout.

With a non-linear closure it is not a priori clear that for each set of boundary conditions there exists a solution that is physically acceptable. Körner & Janka (1992; hereafter KJ) studied

the stationary state problem and proved that physically acceptable solutions must contain a so called critical point (see the following section). Due to this critical point however, they doubted that solutions of steady state two-moment transport could be obtained numerically.

In the following section some of the mathematical properties of the two-moment equations plus a non-linear closure are derived. Treating the closure in the most general form, our approach provides an extension to the analysis of KJ. Furthermore, we give meaning to the critical point within the full time-dependent problem, with the steady state solution as a special case.

Numerical tests are discussed in Sect.3. Using a discrete mesh relaxation method, the steady state two-moment solution is accessed as the end point of a time series. Results are shown for two particular problems: a physical problem of neutrino transport in a hot proto-neutron star and a toy model for which an analytic solution is at hand. For the physical model the two-moment solution is compared with the full solution $F(r, \mu)$ of steady state transport calculated with a Feautrier method. The toy model serves to demonstrate that the two-moment method also works in quite extreme cases, while at the same time it gives an example how the closure can fail to produce the correct diffusive flux. The solutions that we obtain contain a critical point and are stable in the sense that they are not disturbed by the unphysical solutions nearby which diverge from the physical solution away from the critical point.

2. Mathematical properties of two-moment closure

In this section the mathematical character of the set of Eqs. (2)-(3) plus a non-linear closure (5) is investigated. First a short summary of the analysis of KJ is given. Their work is extended to a slightly more general closure, treating the full time-dependent problem. We derive an extra condition on the closure that must be satisfied to guarantee that the two-moment equations are hyperbolic. The closure that we used in our numerical work is described and is shown to satisfy the hyperbolicity requirement.

2.1. Steady state transport: the critical point

KJ investigated steady (=stationary) state problems, i.e. the time-derivatives $\partial_t J$ and $\partial_t H$ in Eqs. (2)-(3) are both zero. They considered the widely used type of closure that expresses the variable Eddington factor $k \equiv K/J$ in terms of the flux ratio $h \equiv H/J$:

$$k = k(h) \quad . \quad (6)$$

With the closure $K = J k(h)$ inserted, and using Eq. (2) to eliminate the $\partial_r H$ term, the momentum balance equation, Eq. (3), can be written as follows:

$$f_1 \partial_r J = f_2 \quad , \quad (7)$$

with

$$f_1 \equiv \partial_J K = k - h \frac{dk}{dh} \quad , \quad (8)$$

and

$$f_2 \equiv -(\kappa_a + \kappa_s)hJ - \frac{(3k-1)}{r}J - \partial_h k \left[\kappa_a(B-J) - \frac{2hJ}{r} \right] \quad . \quad (9)$$

KJ noted that for a given solution $J(r)$, $H(r)$, Eq. (7) develops a singularity at some point $r = r_c$ when $f_1 = 0$, unless the right hand side f_2 also vanishes there. Moreover, for the atmospheric problem, with $\kappa_a(r)$, $\kappa_s(r) \rightarrow 0$ at the surface, they proved that any physically acceptable solution *must* contain a critical point

$$k - h \frac{dk}{dh} = 0 \quad , \quad (10)$$

where f_1 changes sign. Since physical solutions are regular, and not singular, f_2 must also vanish at the critical point r_c . However, their study of the solution topology (for a particular solution) in the neighbourhood of the critical point showed that the critical point is a saddle point. From this it was argued that “*these solutions (the regular ones) turn out to be unaccessible by common discrete mesh methods.*”

2.2. Time-dependent transport: hyperbolicity

We maintain the time-dependence of the two-moment equations and take the closure to be of the general form

$$k = k(J, h) \quad , \quad (11)$$

i.e., the Eddington factor is allowed to depend explicitly on J .

Slightly rewriting the two-moment equations,

$$\partial_t \begin{pmatrix} J \\ H \end{pmatrix} + M \partial_r \begin{pmatrix} J \\ H \end{pmatrix} = \begin{pmatrix} \kappa_a(B-J) - 2H/r \\ -\kappa_{\text{tot}}H - (3K-J)/r \end{pmatrix} \quad , \quad (12)$$

(with $\kappa_{\text{tot}} = \kappa_a + \kappa_s$) shows that the matrix

$$M \equiv \begin{pmatrix} 0 & 1 \\ \partial_J K & \partial_H K \end{pmatrix} \quad (13)$$

multiplying the ∂_r term becomes singular when

$$\partial_J K = 0 \quad . \quad (14)$$

With the two-dimensional closure (11), the function $f_1(r)$, defined as before, becomes

$$f_1 \equiv \partial_J K = k + J \partial_J k - h \partial_h k \quad , \quad (15)$$

and changes sign at some point r_c where

$$k + J \partial_J k - h \partial_h k = 0 \quad . \quad (16)$$

Note that a one-dimensional closure $k(h)$ has $\partial_J k = 0$, so that Eq. (16) reduces to KJ’s definition, Eq. (10), for the critical point. At the critical point r_c the derivative $\partial_r J$ cannot be determined from the two-moment equations (12). In a time-dependent problem, this is of no concern, because it only means

that the subsequent evolution of the radiation field at the critical point does not depend on the specific value of $\partial_r J$. In a steady state the case may be problematic when the solution is to be found by (numerical) integration and the value of $\partial_r J$ is required at every radius r . This is further discussed in Sect.4.

To elaborate on the critical point, it is noted that the two-moment equations describe approximate radiative transport, provided they are of hyperbolic nature. The transport equation is a first order partial differential equation describing an initial value problem. The two moment equations are a set of first order partial differential equations and should also describe an initial value problem. For initial value problems, the appropriate equations to consider are those of hyperbolic type (Garabedian 1964). The system Eq. (12) is hyperbolic when the eigenvalues $\lambda_{1,2}$ of M are both real. For the general closure $K = K(J, H)$, the eigenvalues are

$$\lambda_{1,2} = \frac{1}{2} \partial_H K \pm [(\frac{1}{2} \partial_H K)^2 + \partial_J K]^{\frac{1}{2}} \quad (17)$$

The eigenvalues are real when the discriminant

$$\Delta \equiv (\frac{1}{2} \partial_H K)^2 + \partial_J K \geq 0 \quad (18)$$

At the critical point, the hyperbolic nature of the equations is unchanged, but one of the eigenvalues $\lambda_{1,2}$ of M changes sign: for $\partial_J K > 0$ the eigenvalues are of opposite sign, for $\partial_J K < 0$ they are of the same sign, which is positive if $\partial_H K > 0$. The situation in a steady state stellar atmosphere is as follows: At large depth the diffusion approximation applies. Then $\partial_J K = \frac{1}{3}$ and $\partial_H K = 0$, and the eigenvalues are $\lambda_{1,2} = \pm 1/\sqrt{3}$. Moving outwards, at the critical point, one of the eigenvalues changes sign from negative to positive, and beyond the critical point, in the transparent zones, the eigenvalues have the same, positive, sign. This has important consequences for the outer boundary condition, as will be discussed in Sect.2.3 below. For the proof that physically reasonable solutions of steady state stellar atmospheric problems must contain a critical point we refer to KJ, with the note that their proof also applies to the more general closure Eq. (11) (it simply involves using the more general expression Eq. (15) for f_1 in Eq. (7)).

The nature of the two-moment equations *does* change when the discriminant $\Delta < 0$. The eigenvalues of M become complex and the two-moment equations change into a mixed hyperbolic-elliptic type. This situation is unphysical, because to mathematically (and numerically) handle such equations one must regard the system as a boundary value problem in space time, which is in contradiction with causality (the solution at time t may then depend on the solution in the future, which is quite unacceptable). Numerically, diverging modes may be encountered when it is attempted to solve such equations as an initial value problem. Therefore, we demand that the closure satisfies the hyperbolicity condition Eq. (18).

2.3. Boundary conditions

A solution of the two-moment equations (12) is singled out by providing an initial condition and boundary conditions. The

number of boundary conditions needed depends on the direction of the characteristics of the equations at the boundaries of the system. The direction of the characteristics in (r, t) space is determined by the sign of the eigenvalues $\lambda_{1,2}$ of the matrix M . A positive eigenvalue belongs to a characteristic along which information can be propagated in the forward radial direction, to larger radii, while a negative eigenvalue is associated with a characteristic that points inwards. In the region where the eigenvalues are both positive, information can only propagate outwards. At the boundaries, the number of boundary conditions that must be specified is equal to the number of characteristics pointing into the system. At the lower boundary, at $r = 0$, one condition must be supplied, because one characteristic is entering the system. Spherical symmetry demands

$$H(r = 0, t) = 0 \quad (19)$$

When a critical point is present, both characteristics are leaving the system at the outer boundary $r = R_{\text{OB}}$ and none enter the system. Therefore there is no need (nor room) for an outer boundary condition.

Ideally, at the outer boundary we would like to maintain conditions in agreement with those imposed on the full transport equation, Eq. (1), for which the incoming radiation at the outer boundary $r = R_{\text{OB}}$ must be specified. We have in mind the outer boundary condition which states that there is no incoming radiation at the surface:

$$F(R_{\text{OB}}, \mu, t) = 0 \quad , \mu < 0 \quad (20)$$

Unfortunately, this angular information can in no way be exactly translated into unique conditions on J, H or K . At best integral formulations of Eq. (20) may be formulated, as expressed by Marshak or Mark boundary conditions, with a freedom to choose the angular weight function (Pomraning 1973; see also the discussion in Sect.IV of Levermore & Pomraning 1981). Therefore, even if an outer boundary condition *would* be allowed, we would not know exactly what to impose there. Fortunately, we don't have to break our head over this problem, because there isn't anything to impose at all. How we dealt with this numerically is explained in Appendix A.

2.4. Maximum entropy closure

The maximum entropy Fermi-Dirac closure (MEC-FD) is a specific closure relation for fermionic radiation. It was designed for neutrino transport in supernova phenomena and we shall use it in our computation of the neutrino radiation field inside a cooling neutron star. The explicit form of MEC-FD was derived and discussed by Cernohorsky & Bludman (1994), and is given by

$$k_{\text{MEC}}(J, h) = \frac{1}{3} + \frac{2}{3} (1 - J) (1 - 2J) \chi\left(\frac{h}{1 - J}\right) \quad , \quad (21)$$

where

$$\chi(x) = 1 - 3x/q(x) \quad , \quad (22)$$

with $q(x)$ the inverse of the Langevin function $x = \coth q - 1/q$. The lowest-order polynomial approximation to Eq. (22), which

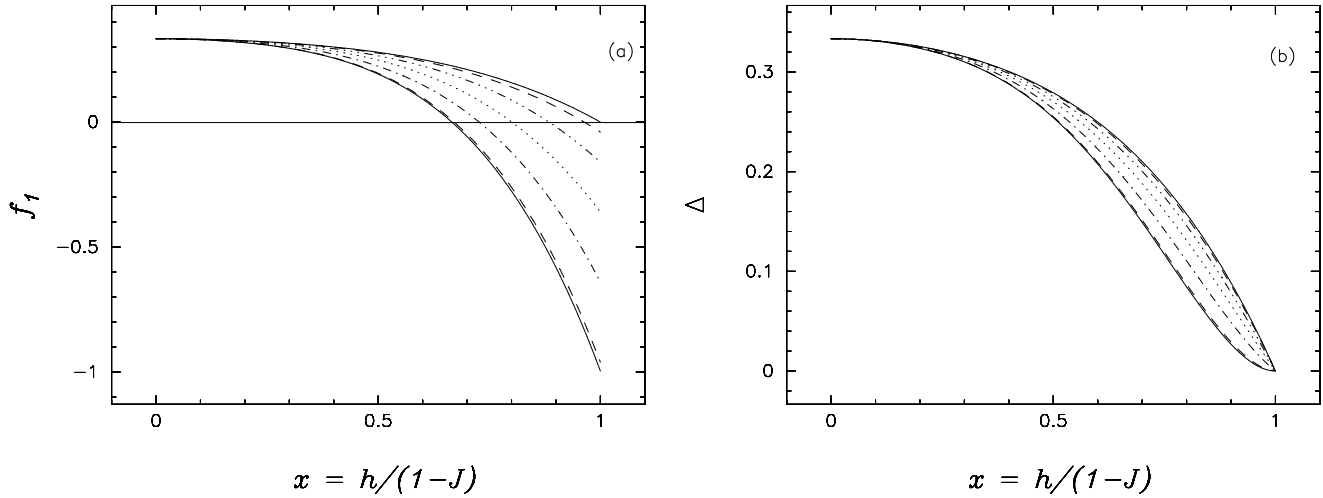


Fig. 1. **a** The quantity $f_1 = \partial_J K$ as function of flux saturation $x \equiv h/(1-J)$, for, from bottom to top, $J = 0.001$ (full line); $J = 0.01$, $J = 0.99$ (dashed); $J = 0.1$, $J = 0.9$ (dash-dotted); $J = 0.2$, $J = 0.8$ (dotted); $J = 0.3$, $J = 0.7$; $J = 0.4$, $J = 0.6$; and $J = 0.5$ (solid, top). **b** The discriminant Δ for the same J -values.

has the correct behaviour in the free-streaming and diffusive limits and contains no free parameters, is

$$\chi(x) = x^2(3 - x + 3x^2)/5 \quad (23)$$

It is accurate to 2% and because of its simplicity has been used in the numerical experiment instead of the exact expression Eq. (22).

Without going into the details and properties of the maximum entropy closure, for which the reader is referred to Janka et al. (1992) and Cernohorsky & Bludman (1994), it suffices to note here that MEC-FD takes into account the Fermi-Dirac quantum statistics of the neutrino radiation, in particular the exclusion principle which for a given occupation density $0 \leq J \leq 1$ limits the flux ratio $h \leq 1 - J$ and the variable Eddington factor $k \leq 1 - 2J + (4/3)J^2$.

To show that $\partial_J K$ changes sign in MEC-FD, the quantity f_1 , defined by Eq. (15), is plotted as a function of flux saturation $x \equiv h/(1-J)$ in Fig. 1a. Due to a symmetry property of MEC-FD which we do not further discuss, the curves of J and $1 - J$ are identical. As occupation density decreases, for $J \neq 0.5$ there is always a value of x for which f_1 changes sign, whereas for $x < 2/3$ it is positive for any J . Moving outward in the atmosphere of, say, a cooling neutron star, the mean free path increases, the occupancy J decreases and h increases, so that f_1 generally changes sign somewhere within the star. Therefore, a MEC-FD solution -if it can be found- will be in agreement with KJ's requirement that any physical solution of two-moment closure must pass through a critical point. Furthermore, Fig. 1b shows that the maximum entropy closure $k_{\text{MEC}}(J, h)$ has the desirable property that $\Delta \geq 0$, a guarantee that the two-moment equations are at all times hyperbolic. At flux saturation $x = 1$, the discriminant $\Delta = 0$ and as a result the eigenvalues become equal and the characteristics coalesce. This is in marginal agreement with a strict hyperbolicity demand. In

most practical situations, however, maximum packing $h = 1 - J$ occurs at an “infinite” radius where $J \rightarrow 0$ and $h \rightarrow 1$.

In the following section we present numerical calculations of two-moment transport using this closure.

3. Numerical two-moment transport

3.1. Neutrino transport in a hot proto neutron star

We are interested in the steady state solution of the two-moment equations (2)-(3) plus MEC-FD closure Eq. (21), with the opacities $\kappa_a(r)$, $\kappa_s(r)$ and the equilibrium distribution $B(r)$ given functions of stellar radius r .

As a case problem we consider electron-neutrino transport in a hot proto neutron star. The matter background used is the model M0 of Cernohorsky & van Weert (1992). It is a hot proto neutron star with a central density of $\rho_c \approx 4 \times 10^{14} \text{ g cm}^{-3}$.

In ordinary applications of neutrino transport, the analysis is spectral and the radiation field, $J(\omega, r)$, $H(\omega, r)$ and $K(\omega, r)$, is computed at a number NB of discrete neutrino energies ω . Normally, we use NB=30 to cover the energy range $1 < \omega < 250$ MeV. For the present purpose this is not necessary and results will be shown for only one energy bin, somewhat arbitrarily chosen at $\omega = 20.6$ MeV. The radial grid has a zoning of NG=195 grid points.

The numerical solution of the two-moment equations is calculated with a relaxation method, treating the problem as an initial value problem. Starting from an initial radiation field, transport is evolved until a steady state is reached where the contributions of the time-derivatives in the equations have become small with respect to other terms.

The initial condition, $J(r)$ and $H(r)$ at $t = 0$ is constructed as follows. Deep inside, at $\rho > 10^{12} \text{ g cm}^{-3}$, the diffusion limit is applied: $J(r, t = 0) = B(r)$ and $H(r, t = 0) = -\frac{1}{3} \partial_r B / (\kappa_{\text{tot}})$. Further out, for $\rho < 10^{12} \text{ g cm}^{-3}$, the radiation is attenuated

geometrically: $J(r, t = 0) \propto 1/r^2$ and $H(r, t = 0) \propto 1/r^2$. This initial condition is rather artificial, but since we are only interested in the steady state solution, the choice of initial condition is, and should be, immaterial. In Appendix A the specifics of the numerical algorithm and the boundary conditions are outlined.

The two-moment MEC-FD steady state solution is shown in Fig. 2. The figure shows a diffusive region below $r \approx 33$ km surrounded by an extended atmosphere. In the diffusive interior, $k \approx 1/3$. In the semi-transparent regions out to the fully transparent surface, h steadily increases. At the stellar surface $h = 0.87 < 1$, indicating that the physical surface is, loosely speaking, not at infinity, but at some finite distance from the neutrino-sphere (“optical” depth $\tau = 2/3$ occurs at $r = 36.2$ km).

Fig. 3 shows the derivative $f_1(r) \equiv \partial_J K$ as a function of stellar radius along the MEC-FD steady state solution. As anticipated, the derivative changes sign. This occurs near $r_c = 41$ km. Beyond this radius the atmosphere becomes scattering dominated and the luminosity function $H(r) r^2$ levels off, to eventually remain constant at $r > 48$ km. In the same figure the quantity $f_2(r)$, defined in Eq. (9), is drawn. The curves change sign simultaneously, between $40.7 < r_c < 41.0$ km, up to the spatial resolution of the grid.

The solution topology diagram of KJ (their Fig. 1; derived for a pure scattering medium) suggested that near the critical point, the solution should be very sensitive to small perturbations, like round-off errors, because divergent solutions are near to the regular solution. The solution we find is stable in the sense that it is achieved by a smooth relaxation from the initial condition to the steady solution and that in the neighbourhood of the critical point, the functions $J(r)$, $h(r)$ and $k(r)$ are regular and behave normally. To test the stability of the steady state, it was disturbed (inflicting up to 30% random fluctuations on J) in the vicinity of the critical point. The disturbed solution relaxed back into the same steady state. To make sure that the solution is indeed stationary, and that the solution near the critical point is not controlled by the time derivatives, however small they might be, we put the time-derivatives equal to zero by hand in the numerical code and then iterated the solution for another few-thousand times or so. This did not at all affect the solution.

To test the accuracy of the two-moment solution, we also computed the solution $F(r, \mu)$ of the stationary state transport equation (i.e., with the ∂_t term in Eq. (1) left out), using a modified Feautrier method (Mihalas & Mihalas, 1984). The Feautrier method is basically a discrete ordinate method that solves the transport equation, Eq. (1), at a number of discrete μ -values.

The “exact” numerical solution of the transport equation with the Feautrier scheme was obtained using 8 discrete angular zones, in the range $\mu \in [0, \pi]$, which is equivalent to 16 angular zones in the range $\mu \in [-\pi, \pi]$ in an ordinary discrete ordinate method. The angles were chosen to lie at equally spaced μ intervals. The number of radial grid points was $\text{NG} = 195$, as before.

For the outer boundary condition we took no incoming radiation. The accuracy of the two-moment MEC-FD approximation may be inferred by a comparison with the Feautrier solution, also drawn in Fig. 2. In the figure the two-moment and Feautrier so-

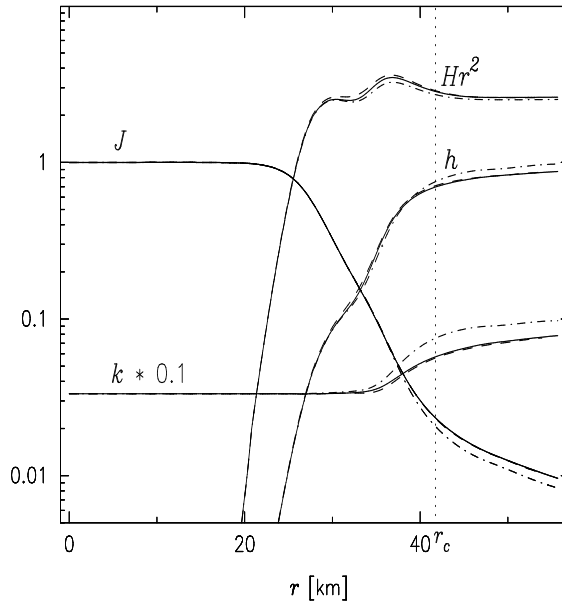


Fig. 2. Steady state solution of electron-neutrino transport. Shown are the occupation density J , the “luminosity” $H r^2$ in units of 0.1 km^2 , the flux-ratio $h \equiv H/J$, and the Eddington factor $k \equiv K/J$ (times 0.1). The two-moment MEC-FD solution is drawn with solid lines, the Feautrier solution with dashed lines. The dash-dotted lines represent the two-moment solution with the Levermore Pomraning closure. The vertical dotted line marks the radius at which the critical point occurs.

lutions of $J(r)$ are indistinguishable. The difference between the two $J(r)$ solutions is in the order of 1% at radii $r > 30$ km, with a largest difference of 1.7% at $r = 35$ km. The difference in the flux H (see $H r^2$ in Fig. 2) is somewhat larger. The two-moment flux deviates by an average factor of 2% for $r < 30$ km, by 7% at $r = 33$ km while the error is smaller than 1% at $r > 40$ km. The same numbers apply to the flux ratio h . The Eddington factor k agrees within 4% at $r = 35$ km and about 2% further out.

To appreciate the accuracy of the two-moment MEC-FD solution, Fig. 2 also shows the two-moment steady state solution that was computed using the Levermore & Pomraning (1981) closure. In parameterised form, the Levermore & Pomraning (LP) closure is given by

$$h = \coth R - 1/R \quad (24)$$

$$k = \coth R (\coth R - 1/R) \quad (25)$$

The closure is of the form $k = k(h)$ and has $f_1 > 0$ for $h \neq 1$ and $f_1 = 0$ at $h = 1$. As pointed out by KJ, a closure with $f_1(h) \geq 0$ must necessarily force the radiation field to $h = 1$ as soon as the opacities drop to zero. This is exactly what is seen in Fig. 2, where the LP solution is drawn with dash-dotted lines. The total neglect of geometry results in a poor approximation at radii $r > 35$ km. This affects not only H , for which the LP solution deviates from the Feautrier solution by more than 10% at $r = 35$ km, but also affects J and the Eddington factor k , which are off by more than 15% and 20%, respectively, in the outer zones of the star.

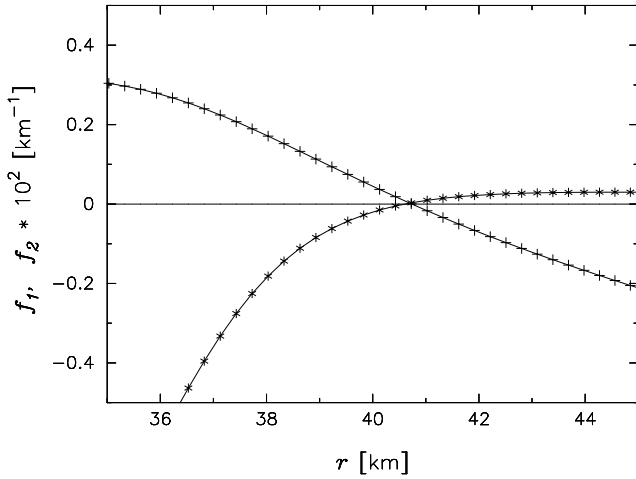


Fig. 3. Quantities $f_1 = \partial_J K(J, h)$, marked with crosses “+”, and f_2 (defined in Eq. (9)) along the MEC solution in a region around the critical point. The markers locate the grid positions.

It is noted that, with our approach, the Feautrier method is actually much faster than the two-moment method in computing the numerical stationary state solution. This is because the transport equation is linear, while the two-moment equations, as a result of the closure (and also because of the necessary choice of J , h and k as dependent variables; see Appendix A) are non-linear. The non-linearity requires an iterative approach to find the stationary state solution. At each of the many time steps in the relaxation process, a set of $3 \times \text{NG}$ equations must be solved simultaneously. To attain a stationary state solution, we typically needed some 1000 time steps or so. The Feautrier steady state solution, on the other hand, can be obtained directly from a single matrix inversion of $\text{NM} \times \text{NG}$ equations, with NM being the number of discrete angular ordinates. Where the two-moment method pays off is in time-dependent problems, where at each time step Δt the radiation field changes by a small amount. The two-moment approach still requires an iterative procedure for convergence to the $t + \Delta t$ solution, but the number, NI , of iterative steps, is usually small (2 or 3). For time dependent problems, the speed of the two-moment method relative to the Feautrier scheme scales roughly as $(\frac{\text{NM}}{3})^2 / \text{NI}$. For example, if we were to compute the time evolution of the radiation field from the initial condition with the Feautrier scheme, in the same way as with the two-moment relaxation method, the computational effort would be larger by this factor.

3.2. The homogeneous sphere

In the previous section the matter background was nicely behaved with the functions $\kappa_a(r)$, $\kappa_s(r)$ and $B(r)$ being relatively smooth functions of stellar radius. As a severe test of the two-moment method plus MEC-FD, we shall investigate a background which is discontinuous. We take $\kappa_s = 0$ and set both $\kappa_a(r) = \kappa = \text{constant}$ and $B = b = \text{constant}$ in a region $r \leq R$, and empty space outside. This homogeneous sphere can be thought of as some sort of isothermal globe of constant den-

sity. The usefulness of this artificial model lies with the fact that the steady state transport problem has a very simple analytic solution:

$$F(r, \mu) = b(1 - e^{-\kappa s(r, \mu)}) \quad , \quad (26)$$

where

$$s = \begin{cases} r\mu + Rg(r, \mu) & r < R, \\ 2Rg(r, \mu) & r \geq R, \end{cases} \quad \begin{matrix} -1 < \mu < +1 \\ [1 - (\frac{R}{r})^2]^{\frac{1}{2}} < \mu < +1 \end{matrix} \quad (27)$$

and

$$g(r, \mu) \equiv [1 - (\frac{r}{R})^2(1 - \mu^2)]^{\frac{1}{2}} \quad . \quad (28)$$

This solution is easily obtained from the formal solution of the transport equation; see e.g. chapter 2 in Duderstadt and Martin (1979).

The first two angular moments of the analytic exact solution are

$$J(r) = b[1 - \int_0^1 d\mu \cosh(\kappa r \mu) e^{-\kappa R g(r, \mu)}] \quad , \quad (29)$$

and

$$H(r) = b \int_0^1 d\mu \mu \sinh(\kappa r \mu) e^{-\kappa R g(r, \mu)} \quad . \quad (30)$$

Deep inside, $r \ll R$, the solution satisfies the diffusion relation

$$H(r) \approx -\frac{1}{\kappa(1 + \frac{2b}{\kappa R})} \frac{\partial J}{\partial r} \quad . \quad (31)$$

The results shown below were obtained for $\kappa = 4$, $b = 0.8$, and $R = 1$. A mesh of $\text{NG}=800$ grid points was used to cover the region $0 \leq r \leq 3$. The problem may be quite simple from a mathematical point of view, but requires a robust numerical algorithm to be able to deal with the discontinuity at $r = 1$, where empty space suddenly begins. It must be noted that the analytic solution (26) makes no distinction between fermionic or bosonic particles whereas the Fermi-Dirac closure used in our two-moment solution formally applies to fermionic radiation only.

The steady state solution of the two-moment equations with the MEC-FD closure is shown in Fig. 4, together with the analytic solution. The integrals (29) and (30) (and a similar integral for K) were computed with a 40-point Gauss-Legendre integration. Also shown again is the two-moment solution with the LP closure. At first sight, the MEC-FD solution seems rather good. The zeroth moment J is approximated with an error that is at worst 10%, which is in the transition region around $r = 1$. The flux-ratio h is also approximated better than 10% at $r > 0.9$, and particularly the way in which the radiation field becomes forwardly peaked is well reproduced. The errors in the LP solution are left unquantified because it is evident in Fig. 4 that LP fails completely: the forward peaking $h \rightarrow 1$ sets in almost immediately where empty space is met, and the resulting errors in J and k are dramatic.

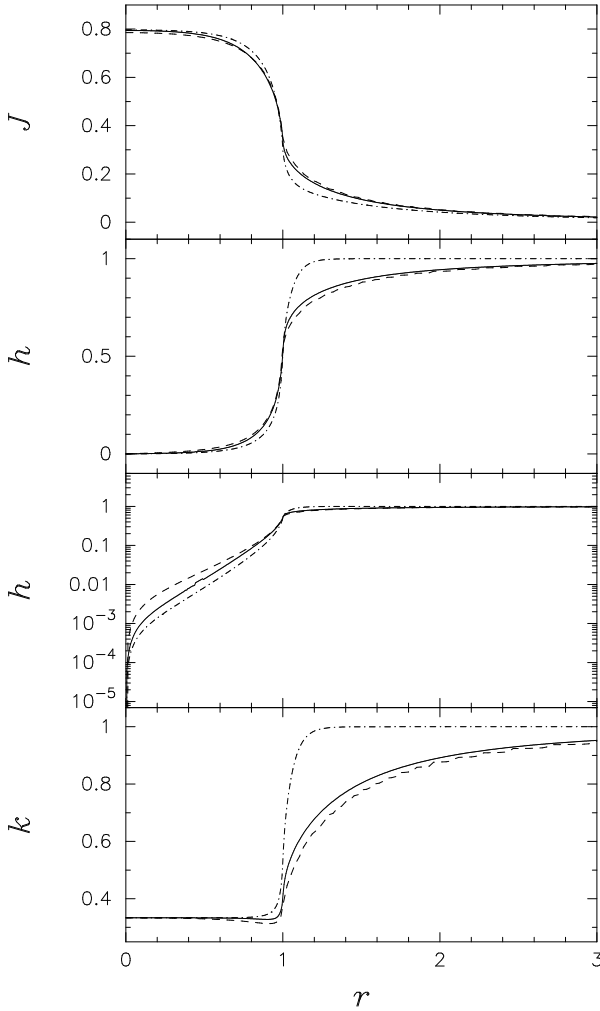


Fig. 4. Steady state solution $J(r)$, $h(r) = H(r)/J(r)$, and $k(r) = K(r)/J(r)$ for the homogeneous sphere problem. Solid lines refer to the two-moment MEC-FD steady state, dashed is the exact solution and dash-dotted is the two-moment LP steady state solution.

However, the logarithmic graph of h in Fig. 4 shows that both MEC-FD and LP fail to produce the correct flux in the diffusive interior. The MEC-FD flux ratio h is wrong by a factor of 2.4 below $r = 0.1$, while the LP flux is even worse. The reason for this discrepancy is that the closures prescribe an incorrect diffusive flux. At large depth, $\frac{2b}{\kappa R} \ll 1$, the exact solution flux H satisfies (see Eq. 31)

$$H(r) = -D \frac{dJ}{dr} \quad , \quad (32)$$

with $D = \frac{1}{\kappa}$. Considering for the moment only the MEC-FD closure, the MEC-FD diffusion approximation is

$$H_{\text{MEC}}(r) = -D_{\text{MEC}} \frac{dJ_{\text{MEC}}}{dr} \quad , \quad (33)$$

with the diffusion coefficient $D_{\text{MEC}} = \frac{1}{3\kappa}$, a factor of three smaller. The closure was designed to take on this limit and forces

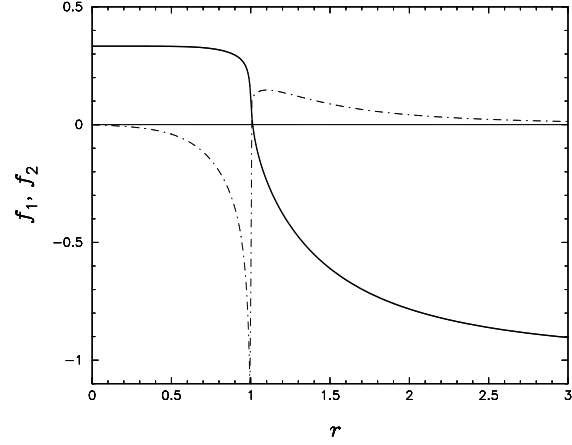


Fig. 5. Quantities $f_1 \equiv \partial_J K(J, h)$ (solid curve) and f_2 (defined in Eq. (9)) along the two-moment solution of the homogeneous sphere.

the solution into this form. Numerical tests showed that the discrepancy becomes larger when κ is increased: when $\kappa=10$, the flux is wrong by several orders of magnitude, much more than may be expected from the factor of three between the diffusion coefficients D and D_{MEC} . This is because the exact solution J and the MEC-FD solution J_{MEC} slightly differ. The difference

$$\Delta(r) \equiv J(r) - J_{\text{MEC}}(r) \quad , \quad (34)$$

may be very small, but it is the *gradient* of this difference that determines the difference between H and H_{MEC} . We can write

$$H/D - H_{\text{MEC}}/D_{\text{MEC}} = \frac{d\Delta}{dr} \quad . \quad (35)$$

This can take on any size, and therefore the difference $H - H_{\text{MEC}}$ is also unlimited. The same argument holds for the LP closure. In practice, this failure of the closure to reproduce the correct diffusive flux will seldom occur, because most physical systems have temperature and chemical gradients that drive fluxes locally. In a homogeneous system there is only one “gradient” that drives the flux: the edge of the system.

Fig. 5 shows the functions $f_1(r)$ and $f_2(r)$ as a function of radius along the MEC-FD steady state solution. Again, both functions change sign at the same point. This occurs at the surface $r = 1$ of the sphere where empty space begins. The function f_2 changes sign discontinuously. This is due to the fact that $\kappa_a(r)$ and $B(r)$ are discontinuous at $r = 1$. Apparently such discontinuities do not pose difficulties that cannot be overcome numerically; the two-moment solution $J(r)$, $h(r)$, $k(r)$ is regular.

4. Discussion

The problem of finding the steady state solution of the two-moment equation using a non-linear closure, is, due to the critical point, similar to stellar wind problems. In stellar wind theory the transonic solution for the wind speed $v(r)$ is searched as the single physically acceptable solution from a haystack

of diverging or otherwise physically unacceptable solutions. In a very simple model of the solar wind (Parker, 1960), the wind speed $v(r)$ is a solution of an ordinary differential equation (ODE) $a(v, r) dv/dr = b(r, v)$. It can be shown that the physically acceptable solution must cross the point $a = b = 0$ at which it changes from sub- to supersonic, in analogy with the functions $f_1(r)$ and $f_2(r)$ changing sign simultaneously in Eq. (7). Finding the critical solution numerically may be difficult if a direct integration method is used because the wind solution topology is of the saddle (or “X”) type. In the so called “shooting” method the wind speed $v(r_0)$ is guessed at the inner boundary and then the ODE is integrated outwards. Even if the correct value $v(r_0)$ were known, the shooting method could never produce the single physically acceptable solution; this would require an infinitely high precision and resolution. All the other solutions diverge from the physical solution, and any small rounding error will push the numerical solution onto one of the unphysical solutions. To be able to access the transonic solution directly, discrete mesh methods are used. For example, the Henyey method, developed to integrate the equations of stellar evolution, has been extended (see, eg., Nobili & Turolla, 1988) as a general tool to solve systems of (non-linear) ordinary differential equations: the equations are placed on a spatial grid and turned into non-linear difference equations which are solved iteratively, starting from an initial guessed solution. Our relaxation process is very similar. At each time step a system of non-linear equations is solved iteratively. The main difference is that with the relaxation process that we use, the initial guess does not need to be close to the steady state solution. As long as the equations are hyperbolic, we are assured that the solution evolves to the steady state (provided the steady state exists). This is the reason that we must impose the hyperbolicity condition Eq. (18) on the closure. For the same reason an arbitrary set of ODEs cannot be solved by simply adding a time-dependent term and solving a time-series; the resulting equations will in general not be hyperbolic.

In stellar wind modelling, the critical point must be carefully dealt with. At the critical point the numerical equations are replaced by continuity conditions. We did not deal with the critical point in such a manner. In fact, we made no special arrangement whatsoever to deal with the critical point. Nevertheless, the solutions we found did contain such a point, within the accuracy that the grid spacing offers. The location of the critical point is not a priori known; it depends on the solution of the two-moment equations. Therefore the critical point will almost never be hit exactly in numerical calculations. But even in the unlikely case it is met, there should be no problem. The discrete mesh method “tries” a solution to fit the equations. At the critical point the derivative is undetermined by the equations, but since the solution is a trial one, the value of the derivative is not inferred from the equations, but from the trial solution itself. If the trial solution is regular, so is the derivative. In time-dependent radiative transport the critical point is even of lesser consequence because then the derivatives are determined by the solution at a previous time step (or at the future time step in an implicit

formulation) and all the derivatives are again determined by the solution.

A final point to address is whether or not a two-moment solution with a critical point is physically acceptable in the sense that the outer boundary condition (OBC) must be given up. This may seem to be at variance with the fact that the transport equation, which we approximate, requires an OBC for the incoming radiation at the outer boundary. The answer is, that using a P-N method as a means to approximate radiative transport has the unpleasant consequence that is impossible to translate the exact OBC uniquely into conditions on the moments of the radiation field. How well the radiation field is approximated by a two-moment solution thus also depends on the particular OBC used in the two-moment method. In this line of reasoning we may interpret the case when there is no OBC at all as yet another way to approximate the true radiation field -and consequently accept the critical solution when the approximation is a good one. At least in one case (Sect.3.1) we demonstrated that the two-moment critical solution was quite accurate.

5. Conclusions

We studied the two-moment (P-1) equations of approximate radiative transfer with the non-linear Maximum-Entropy closure for Fermi-Dirac statistics.

For spherically symmetric atmosphere problems it can be shown that physically reasonable steady state solutions will go through a critical point (Körner & Janka 1992), similar to the critical points encountered in the theory of stellar winds. This critical point has no physical meaning but can be mathematically well understood. Such an understanding is important since the existence of such a critical point has severe implications on the way that boundary conditions determine which solution will be found. We have performed a mathematical and numerical study of these aspects and demonstrated that the two-moment equations with a Fermi-Dirac Maximum Entropy closure contain a critical point, are well behaved, and that the solutions are physically acceptable, regular and, in one example, accurate.

We conclude that the two-moment P-1 approach with non-linear closures for which $\partial_j K$ changes sign can be formulated in a numerically stable fashion, provided that the closure satisfies the hyperbolicity demand Eq. (18). In particular this allows the use of closures that incorporate forward peaking in systems where an opaque interior is surrounded by a transparent atmosphere.

Acknowledgements. JMS is grateful to R. Takens for discussing at length various aspects of radiative transport and to S.M. Verduyn-Lunel for his comments on the mathematical part. We would like to thank L.J. van den Horn and Ch.G. van Weert for their comments and suggestions.

Appendix A: numerical approach

This section provides a description of the numerical algorithm used to solve the two-moment equations. The two-moment equations, Eqs. (2+3) plus the closure Eq. (5), were solved for

J , the flux ratio $h = H/J$ and the Eddington factor $k = K/J$. These have the convenient property that their magnitudes are limited, whereas the size of H and K is unlimited. With Eq. (2) substituted in (3) to get rid of the $h\partial_t J$ -term, the momentum balance equation is rewritten as

$$J\partial_t h + \frac{1}{r^2}\partial_r(r^2 Jk) - \frac{h}{r^2}\partial_r(r^2 Jh) + \frac{(k-1)}{r}J + h(\kappa_a B + \kappa_s J) = 0 \quad . \quad (\text{A1})$$

This rearrangement is adopted from flux limited diffusion theory (Levermore, 1984), where the momentum-balance equation, Eq. (3), is written as (Janka, 1991):

$$\frac{h}{k-h^2} = -\frac{\partial_r \ln J}{\kappa_a B/J + \kappa_s + \Xi} \quad , \quad (\text{A2})$$

with the artificial opacity defined as

$$\Xi \equiv \frac{1}{h} [\partial_t h + \partial_r k - h\partial_r h + (3k-1-h^2)/r] \quad . \quad (\text{A3})$$

The choice of using J , k and h instead of J , H and K as dependent variables, plus the rearrangement of the momentum balance equation in the form of Eq. (A1) above, were found to be essential for obtaining a numerically stable algorithm; all numerical attempts dealing directly with the set Eqs. (2)-(3) were in vain.

Eqs. (2) and (A1) are placed on a discrete grid of $\text{NG} - 1$ discrete cells surrounded by NG cell-surfaces. Scalar quantities and tensors of even rank ($J_{i+\frac{1}{2}}, k_{i+\frac{1}{2}}, \kappa_{i+\frac{1}{2}}$) are cell-centered, vectors (h_i, r_i) are on the cell-surface. Cell $i + \frac{1}{2}$ is enclosed by the cell-surfaces i and $i + 1$.

The discrete, fully implicit formulation of Eq. (2) is strictly conservative:

$$\begin{aligned} & \frac{1}{\Delta t}(J_{i+\frac{1}{2}}^{n+1} - J_{i+\frac{1}{2}}^n) + \\ & \frac{1}{V_{i+\frac{1}{2}}}(A_{i+1}[J^{n+1}]_{i+1}h_{i+1}^{n+1} - A_i[J^{n+1}]_i h_i^{n+1}) - \\ & (\kappa_a)_{i+\frac{1}{2}}(B_{i+\frac{1}{2}} - J_{i+\frac{1}{2}}^{n+1}) = 0 \quad , \quad i = 1, \text{NG} - 1 \quad , \quad (\text{A4}) \end{aligned}$$

with A_i the area of shell r_i and $V_{i+\frac{1}{2}}$ the volume enclosed by shells r_i and r_{i+1} . The finite difference form of (A1) is “almost” conservative:

$$\begin{aligned} & [J^{n+1}]_i \frac{1}{\Delta t}(h_i^{n+1} - h_i^n) + \\ & \frac{1}{[V]_i} \{ \langle A \rangle_{i+\frac{1}{2}} J_{i+\frac{1}{2}}^{n+1} (k_{i+\frac{1}{2}}^{n+1} - h_i^{n+1} \langle h^{n+1} \rangle_{i+\frac{1}{2}}) - \\ & \langle A \rangle_{i-\frac{1}{2}} J_{i-\frac{1}{2}}^{n+1} (k_{i-\frac{1}{2}}^{n+1} - h_i^{n+1} \langle h^{n+1} \rangle_{i-\frac{1}{2}}) \} + \\ & [J^{n+1} (k^{n+1} - 1)]_i / r_i + [\kappa_a B + \kappa_s J^{n+1}]_i h_i^{n+1} = 0 \quad , \\ & i = 2, \text{NG} - 1 \quad . \quad (\text{A5}) \end{aligned}$$

Finally, the closure in the form Eq. (11) is solved as it stands

$$k_{i+\frac{1}{2}}^{n+1} = k(J_{i+\frac{1}{2}}^{n+1}, h_i^{n+1}) \quad , \quad i = 1, \text{NG} \quad . \quad (\text{A6})$$

In these equations a cell centered quantity is placed on the surface by

$$[x]_i = \frac{1}{2}(x_{i+\frac{1}{2}} + x_{i-\frac{1}{2}}) \quad , \quad (\text{A7})$$

and a cell-surface quantity is centered by

$$\langle y \rangle_{i+\frac{1}{2}} = \frac{1}{2}(y_{i+1} + y_i) \quad . \quad (\text{A8})$$

Equation (A4) requires $[J]_{\text{NG}}$, which in turn needs $J_{\text{NG}+\frac{1}{2}}$, which is not at hand. We set $J_{\text{NG}} = \alpha J_{\text{NG}-1} + (1-\alpha)J_{\text{NG}-2}$ with $0.5 < \alpha < 1$. The precise value of α was found to be irrelevant.

Two boundary conditions are required. At the inner boundary condition we impose Eq. (19) in discrete form:

$$h_1^n = 0 \quad . \quad (\text{A9})$$

It was explained in Sect.2.3 that when the solution contains a critical point, there is no room for an outer boundary condition. Nevertheless, the equations above require an extra equation at $i = \text{NG}$ or they cannot be solved. This is not a discrepancy. It only demands that what we do at $i = \text{NG}$ must respect the fact that the characteristics point outwards at the outer boundary. The “virtual” outer boundary conditions (VOBC) that we used in this work is

$$J_{\text{NG}-1}^n h_{\text{NG}}^n r_{\text{NG}}^2 = J_{\text{NG}-2}^n h_{\text{NG}-1}^n r_{\text{NG}-1}^2 \quad , \quad (\text{A10})$$

a sort of staggered flux-conservation. Several other VOBCs were tried (like $h_{\text{NG}} = h_{\text{NG}-1}$), all of which involved some kind of extrapolation. The particular choice affected only the solutions in the last few grid points by a few per mille. We even tried setting $h_{\text{NG}} = 1$. The steady state solutions that were obtained for this VOBC have $h(r)$ exactly as before but with an almost discontinuous jump to $h(r) = 1$ in the last few grid points.

Eqs. (A4), (A5) and (A6), along with the inner boundary condition (A9) and the VOBC (A10) were solved simultaneously at each time step $t^n \rightarrow t^{n+1}$ using a Newton-Raphson procedure until the solution J^{n+1} , h^{n+1} , k^{n+1} had converged at all grid points.

References

- Cernohorsky, J., Bludman, S.A., 1994, ApJ 433, 205.
 Cernohorsky, J., van Weert, Ch.G., 1992, ApJ 198, 190.
 Duderstadt, J.J., Martin, W.R., 1979, Transport Theory. John Wiley & Sons, New York.
 Garabedian, P.R., 1964, Partial Differential Equations. John Wiley & Sons, New York.
 Janka, H.-Th., Dgani, R., van den Horn, L.J., 1992, A&A 265, 345.
 Körner, A., Janka, H.-Th., 1992, A&A 266, 613.
 Levermore, C.D., Pomraning, G.C., 1981, ApJ 248, 321.
 Levermore, C.D., 1984, JQSRT 31, 149.
 Mihalas D., Mihalas W., 1984, Foundations of Radiation Hydrodynamics. Oxford University Press.
 Nobili, L., Turolla, R., 1988, ApJ 333, 248.
 Parker, E.N., 1960, ApJ 132, 821.
 Pomraning, G.C., 1973, The equations of radiation hydrodynamics. Pergamon press, Oxford.

This article was processed by the author using Springer-Verlag L^AT_EX A&A style file L-AA version 3.